



HAL
open science

Study of oxide/metal/oxide thin films for transparent electronics and solar cells applications by spectroscopic ellipsometry

Mihaela Girtan, Laura Hrostea, Mihaela Boclinca, Beatrice Negulescu

► **To cite this version:**

Mihaela Girtan, Laura Hrostea, Mihaela Boclinca, Beatrice Negulescu. Study of oxide/metal/oxide thin films for transparent electronics and solar cells applications by spectroscopic ellipsometry. *AIMS Materials Science*, 2017, 4 (3), pp.594 - 613. 10.3934/matiersci.2017.3.594 . hal-01741580

HAL Id: hal-01741580

<https://hal.science/hal-01741580>

Submitted on 22 Apr 2021

HAL is a multi-disciplinary open access archive for the deposit and dissemination of scientific research documents, whether they are published or not. The documents may come from teaching and research institutions in France or abroad, or from public or private research centers.

L'archive ouverte pluridisciplinaire **HAL**, est destinée au dépôt et à la diffusion de documents scientifiques de niveau recherche, publiés ou non, émanant des établissements d'enseignement et de recherche français ou étrangers, des laboratoires publics ou privés.

Research article

Study of oxide/metal/oxide thin films for transparent electronics and solar cells applications by spectroscopic ellipsometry

Mihaela Girtan^{1,*}, Laura Hrostea^{1,2}, Mihaela Boclinca^{1,2}, and Beatrice Negulescu³

¹ Photonics Laboratory, Angers University, 2, Bd. Lavoisier, 49045, Angers, France

² Faculty of Physics, “Al.I.Cuza” University, Iasi, Romania

³ François Rabelais University, Tours, France

* **Correspondence:** Email: mihaela.girtan@univ-angers.fr.

Abstract: A comprehensive study of a class of Oxide/Metal/Oxide (Oxide = ITO, AZO, TiO₂ and Bi₂O₃, Metal = Au) thin films was done by correlating the spectrophotometric studies with the ellipsometric models. Films were deposited by successive sputtering from metallic targets In:Sn, Zn:Al, Ti and Bi in reactive atmosphere (for the oxide films) and respective inert atmosphere (for the metallic Au interlayer films) on glass substrates. The measurements of optical constants n —the refractive index and k —the extinction coefficient, at different incident photon energies for single oxide films and also for the three layers films oxide/metal/oxide samples were made using the spectroscopic ellipsometry (SE) technique. The ellipsometry modelling process was coupled with the recorded transmission spectra data of a double beam spectrophotometer and the best fitting parameters were obtained not only by fitting the n and k experimental data with the dispersion fitting curves as usual is practiced in the most reported data in literature, but also by comparing the calculated the transmission coefficient from ellipsometry with the experimental values obtained from direct spectrophotometry measurements. In this way the best dispersion model was deduced for each sample. Very good correlations were obtained for the other different thin films characteristics such as the films thickness, optical band gap and electrical resistivity obtained by other measurements and calculation techniques. The ellipsometric modelling, can hence give the possibility in the future to predict, by ellipsometric simulations, the proper device architecture in function of the preferred optical and electrical properties.

Keywords: transparent electrodes; solar cells; ellipsometry models

1. Introduction

ITO (Indium Tin Oxide) is a critical raw material mostly used as transparent electrode [1–6] in many applications such as plastic electronics, flexible solar cells, screens, etc. The huge development of these technologies and the limited resources of Indium require the replacement or the reduction of the necessary quantity ITO for such kind of applications [7–16].

We showed in our previous studies [17] that the quantity of ITO can be divided by four if the ITO films (150 nm) are replaced by ITO (20 nm)/metal (7 nm)/ITO (20 nm) films by maintaining the same figures of merit of the electrodes as that one's of single layer films. Moreover, subsequent studies of Kubis [18] and Berny [19] show the excellent mechanical properties and robustness of these films for large scale applications.

At present the research on founding alternative transparent conducting films for the replacement of ITO is mostly done by many experimental trials. Ellipsometry is a non-destructive, non-invasive non-contact, very precise, reproducible and very sensitive technique for study the ultra-thin films. Spectroscopic ellipsometry (SE) provides a widely applicable method for determining accurate characterization of optical and electrical transport properties of thin films multi-layers structures, in particularly when the multilayer of device structure, is of critical importance to their effective implementation [20,21].

However, the difficulty consists to discern between two or more ellipsometric models which both fits well the same data. In the most reported data in literature, the ellipsometric models studied are considered enough good if the experimental data of the global refractive index (n) and extinction coefficient (k) fits well with the dispersion curves. Nevertheless we remarked for a large number of our experiments and data, that models which fits well with the experimental data for the global n and k they are not necessarily consistent with the other optical parameters, such as the transmission or reflection coefficient.

The purpose of this article is to provide a comprehensive study of the spectroscopic ellipsometric measurements of single oxide films and oxide/metal/oxide multi-layers thin film using a two-modulator generalized ellipsometer by continuing the study much further than usual given in literature and by also comparing the calculated the transmission coefficient from ellipsometry with the experimental values obtained from direct spectrophotometry measurements. This procedure allows establishing in a more accurate way the best dispersion model for each sample.

Given the fact that the characterization of optical and electrical properties of transparent oxide thin films such as ITO, ZnO:Al (Aluminium doped Zinc Oxide—AZO), TiO₂, Bi₂O₃ or multi-layers thin films Oxide/Au/Oxide of the above mentioned oxide is of considerable interest in multiple applications [22–43], we compare the results of multiple techniques for correlating all these properties.

The good correlations obtained between the electrical and optical properties determined experimentally by different techniques and the electrical and optical characteristics obtained by theoretical ellipsometric simulations, indicate that high accurate ellipsometric modelling approach, can give the possibility in the future to predict the appropriate device architecture in function of the desired optical and electrical properties.

2. Materials and Method

The oxide thin films were deposited on glass substrates by sputtering in reactive atmosphere using In:Sn (90%:10%), Zn:Al (98%:2%), Ti and Bi metallic targets from Kurt Lesker and respectively Mateck for the last two. The gold interlayer thin film for the oxide/metal/oxide multi-layers films was deposited in argon atmosphere. The substrates were placed in a vertical target-substrate configuration onto a rotating disk kept at room temperature. The target-substrate distance was of about 70 mm. The deposition parameters are given in Table 1. The deposition rates were 12 nm/min for ITO films, 10 nm/min for AZO films, 7.5 nm/min for TiO₂ thin films, 30 nm/min for Bi₂O₃ thin films and 30 nm/min for gold films. The optimized values of the films thickness were chosen in correlation with literature data and in the range for which we obtained, after many trials, simultaneously good optical and electrical properties. The glass substrate thickness was of 1.1 mm and the refractive index $n = 1.52$.

Table 1. Samples deposition conditions.

Layer	Target composition	Atmosphere conditions	Target-Substrate distance (cm)	Deposition current (mA)	Pressure (10^{-2} mbar)	Deposition time (s)
ITO	In 90%, Sn 10%	Reactive atm.	7	30	2	160
Au	Au 100%	Argon atm.	7	30	1	14
ITO	In 90%, Sn 10%	Reactive atm.	7	30	2	160
ZnO	Zn 98%, Al 2%	Reactive atm.	7	100	2	160
Au	Au 100%	Argon atm.	7	30	1	14
ZnO	Zn 98%, Al 2%	Reactive atm.	7	100	2	160
TiO ₂	Ti 100%	Reactive atm.	7	100	2	160
Au	Au 100%	Argon atm.	7	30	1	14
TiO ₂	Ti 100%	Reactive atm.	7	100	2	160
Bi ₂ O ₃	Bi 100%	Reactive atm.	7	30	2	160
Au	Au 100%	Argon atm.	7	30	1	14
Bi ₂ O ₃	Bi 100%	Reactive atm.	100	30	2	160

Films thickness measurements were done by profilometry using a Dektak profilometer and as well by ellipsometry. The total thickness of oxide/metal/oxide multi-layer structures ranged between 60 and 300 nm.

Samples structures were investigated by X-ray diffraction (XRD) using D8 Advance Bruker diffractometer CuK α 1.2 ($\lambda = 1.5406 \text{ \AA}$), equipped with a linear Vantec super speed detector and by scanning electron microscopy (SEM) using a JEOL microscope.

Optical properties studied were made on single layer oxide thin film and also oxide/Au/oxide three layers films. The investigations of optical properties were made by spectroscopic ellipsometry (SE) technique using a UVVISELTM ellipsometer from Horiba Jobin Yvon, with a 75 W high discharge Xe lamp in the spectral range from 260 to 2100 nm. All the spectra were recorded at room temperature, at an incident angle of 70°. The configuration chosen for the modulator (M), analyzer (A) and polarizer (P) positions were: M = 0°, A = 45° respectively. After the relatively fast recording of ψ and Δ spectra, the next step was the construction of an appropriate optical model for the samples

in order to fit the experimental values. These investigations were coupled with the recording of absorption/transmission spectra using a double beam spectrophotometer LAMBDA 950 UV/Vis/NIR spectrophotometer in the same spectral range from 260 to 2100 nm.

3. Results and Discussions

Figure 1 present the architecture of the studied samples oxide and oxide/metal/oxide deposited on glass substrates and Figure 2 present the SEM micrographs for single oxide layers (named here bottom layer) and then of subsequently oxide layers of the structure oxide/Au/oxide (named top layer). Surfaces are smooth and, generally, small differences were observed between the surface morphology of bottom oxide layer and top oxide layer.

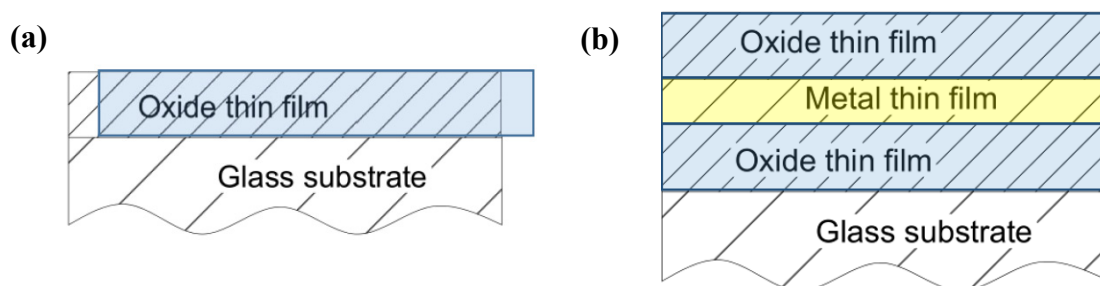


Figure 1. Studied samples architecture.

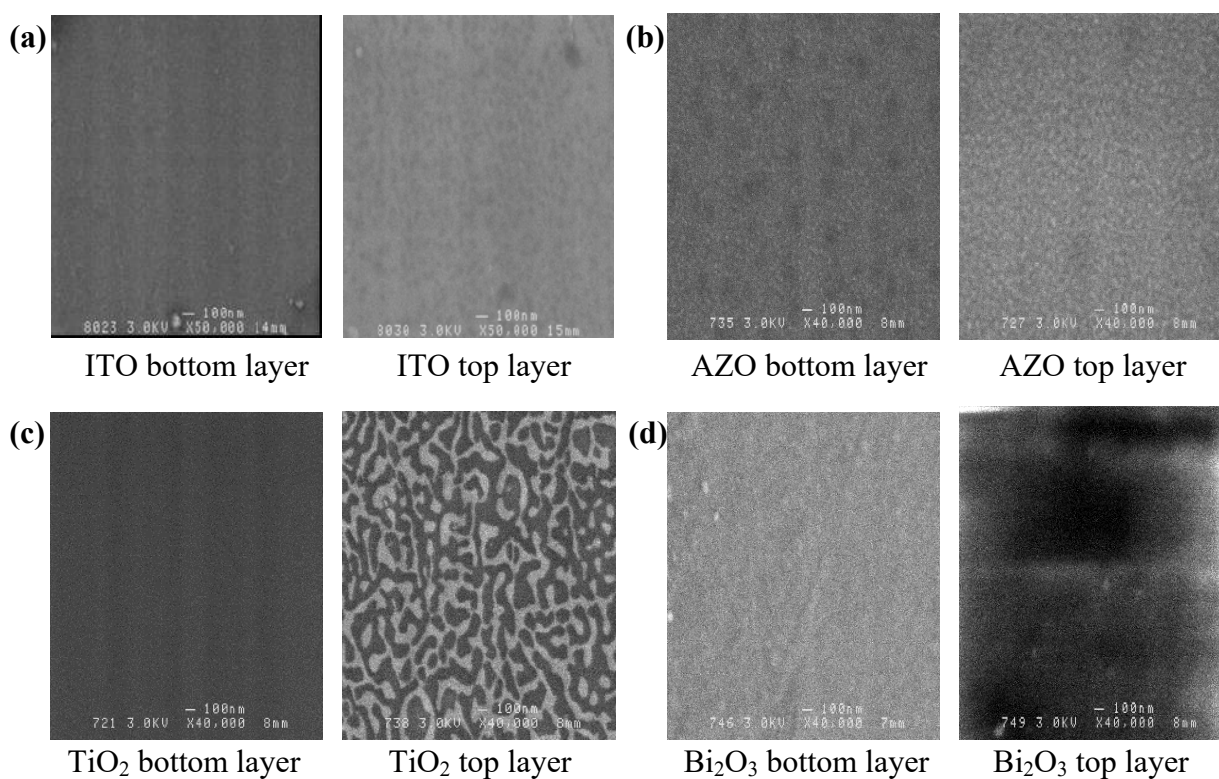


Figure 2. SEM micrograph of oxide single layer (bottom layer) and oxide/metal/oxide samples bottom and top layer: (a) ITO/Au/ITO, (b) AZO/Au/AZO, (c) TiO₂/Au/TiO₂, (d) Bi₂O₃/Au/Bi₂O₃.

The apparently phase-separation like morphology for the $\text{TiO}_2/\text{Au}/\text{TiO}_2$ sample can be attributed to the fact that the top TiO_2 film is very thin, much thinner, compared to the other samples, hence due to the scanning electron microscopy penetration depth, the top image of the three layer sample, the partially image of the gold layer can be visible through the top layer. From other analysis like AFM (not shown here), we did not remark significant differences on the morphology of the top oxide layer compared to the bottom layer.

Figures 3(a–d) show the X-ray diffraction patterns of as deposited oxide single layers films and oxide/metal/oxide films. As one can see all single oxide layers are amorphous. The oxide/metal/oxide layers are also amorphous except AZO/Au/AZO sample which shows small peak corresponding to (002) crystalline plane of ZnO zincite (JCPDS card No. 003-0752), this indicating a preponderantly microcrystalline growth with the (002) plane parallel to the substrate surface. For $\text{TiO}_2/\text{Au}/\text{TiO}_2$ the peak appearing in the XRD pattern (Figure 3c) corresponds to Au (100) crystalline plane (JCPDS card No. 00001-1172). For Bi_2O_3 and $\text{Bi}_2\text{O}_3/\text{Au}/\text{Bi}_2\text{O}_3$ samples, the strongest line corresponds to the (201) plane of the $\beta\text{-Bi}_2\text{O}_3$ phase according to JCPDS card No. 00-027-0050.

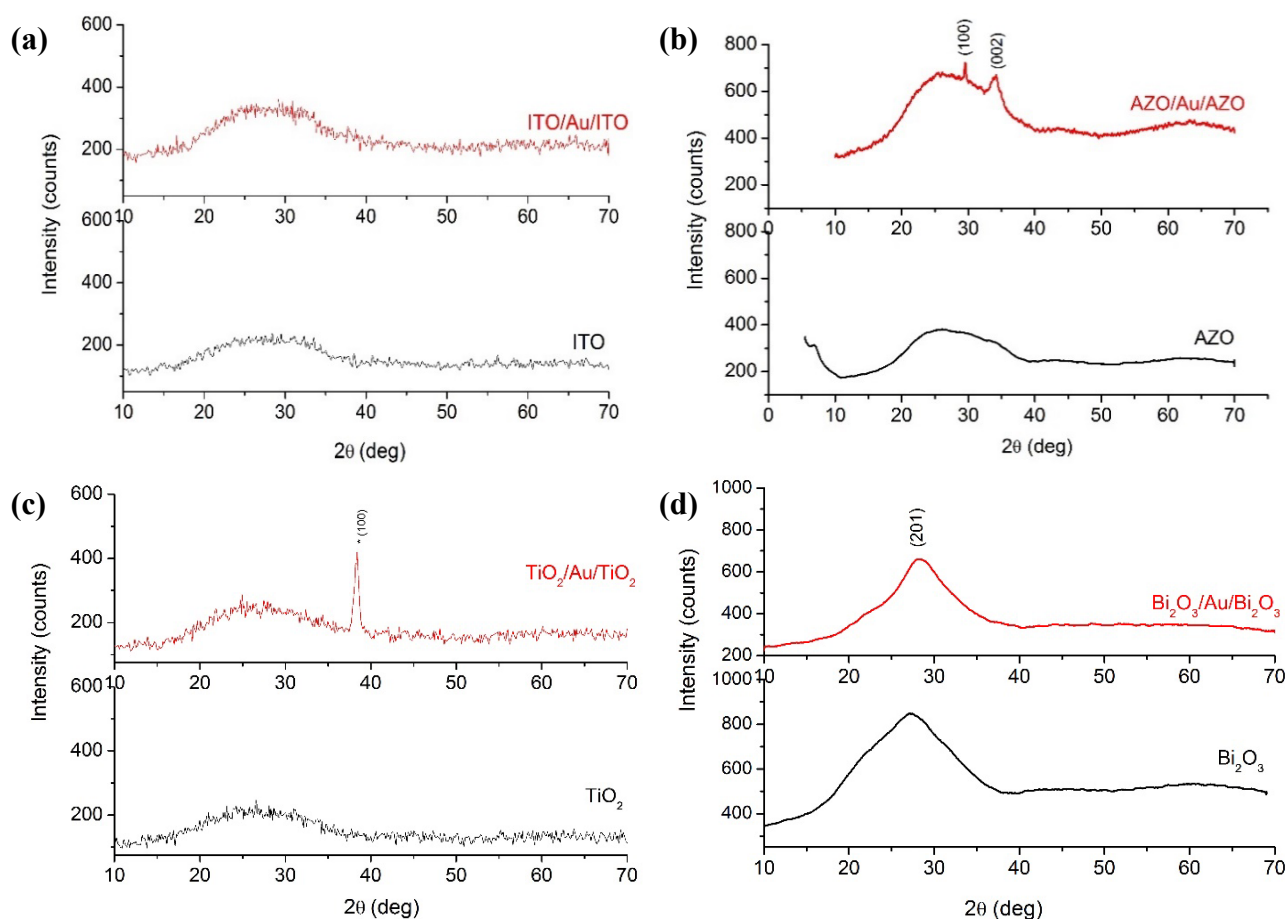


Figure 3. XRD diffraction patterns for (a) ITO single layer and ITO/Au/ITO three layer sample, (b) AZO single layer and AZO/Au/AZO three layer sample, (c) TiO_2 and $\text{TiO}_2/\text{Au}/\text{TiO}_2$, (d) Bi_2O_3 and $\text{Bi}_2\text{O}_3/\text{Au}/\text{Bi}_2\text{O}_3$.

In ellipsometry, the variation of the amplitude and the phase difference between the perpendicular (p) and the parallel (s) components of the reflected light polarized, with respect to the

plane of incidence, are measured. In general, reflection causes a change in the relative phase of p and s waves and in the ratio of their amplitudes. According to the fundamental equation of ellipsometry the relation between the ellipsometric angles ψ and Δ is given by [44]:

$$\tan \psi \exp(i\Delta) = \frac{R_p}{R_s} \quad (1)$$

where, R_p/R_s is the complex ratio of the Fresnel reflection coefficients. ψ —measure the amplitude ratio and Δ —measure the relative phase change.

The measured ellipsometric spectra are fitted by minimizing the squared difference χ^2 between the measured and calculated values of the ellipsometric parameters I_s and I_c . I_s and I_c are given by:

$$I_s = \sin 2\psi \sin \Delta \quad (2)$$

$$I_c = \sin 2\psi \cos \Delta \quad (3)$$

and

$$\chi^2 = \left[\frac{1}{(2N - P)} \right] \sum_i^N [(I_{si}^{exp} - I_{si}^{cal})^2 + (I_{ci}^{exp} - I_{ci}^{cal})^2] \quad (4)$$

where, N is the number of data points and P the number of model parameters [45]. A fit is considered enough good if $\chi^2 < 10$. Ellipsometry is an indirect method. The difficulty is that one that is not sufficient to obtain a good fit of ψ and Δ spectra with very low values of χ^2 . Many dispersion models can fits well and the difficulty is to know what model is the most suitable. That means that once a model is tested and a good fit is obtained the results should be compared with other data measurements and the model should be improve until a good coherence between all the data is obtained. For this reason we conduct our study furthermore than usually presented in literature, by comparing the transmittance spectra calculated from ellipsometry with the transmittance spectra obtained by direct measurements from spectrophotometry.

The refractive index and extinction coefficient for a bulk (substrate) material are related to ψ and Δ by the following formula and can be calculated directly by separating the real and imaginary part of this equation and solving the two equation system [46].

$$\tilde{\varepsilon} = \varepsilon_1 + i\varepsilon_2 = \tilde{n}^2 = (n + ik)^2 = \sin(\theta)^2 \left[1 + \tan(\theta)^2 \left(\frac{1 - \tan(\psi) e^{i\Delta}}{1 + \tan(\psi) e^{i\Delta}} \right)^2 \right] \quad (5)$$

The DeltaPsi2 software of Horiba Jobin Yvon allows to fit the spectra of ψ and Δ , I_s and I_c by minimizing the values of χ^2 . The software calculates also a “global” refractive index and a “global” extinction coefficient of the samples including the substrate + layer(s) and allows to calculate the global transmittance ($T\%$) and reflectance ($R\%$). The individual refractive index, n , and individual extinction coefficient, k , for each layer should be extracted from the model on the basis of the dispersion formula which gives the best fit.

The direct measurement of n and k on the basis of Eq. (5) can be compared with the theoretical values given by the known dispersions models (Adachi-Forouhi, Cauchy, Tauc-Lorentz, Kato-Adachi, Sellmeier, etc.) of different materials from the data basis of the DeltaPsi2 software, and good fits between the measured n and k and calculated n (n -fit) and k (k -fit) can be obtained, for more than one dispersion model.

The theoretical spectral transmittance (T) and reflectance (R) of a thin film deposited on a substrate are functions of n , k , d and λ , where d is the film thickness and λ the wavelength of incident light. The certainty of the appropriate model is achieved when the calculated values T , R and d coincides with the direct measured values of T_{ex} , R_{ex} and d_{ex} , from spectrophotometry for T_{ex} , R_{ex} and profilometry, SEM or other methods for d_{ex} [47]:

$$T(n, k, d, \lambda) = T_{ex}$$

$$R(n, k, d, \lambda) = R_{ex}$$

$$d = d_{ex} \quad (6)$$

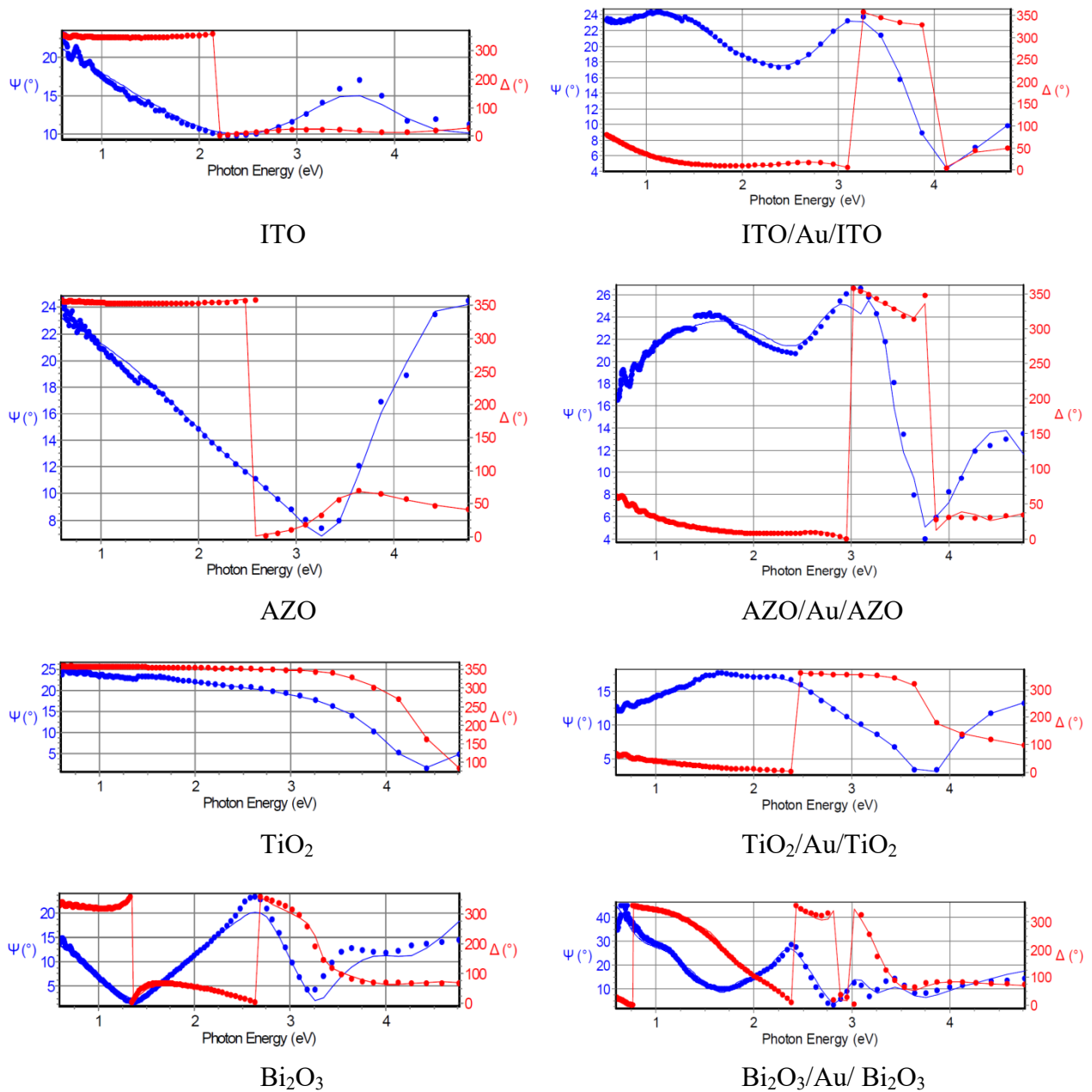


Figure 4. Best fits between the experimental measurements of ellipsometric angles and (dots) and calculated values (line) using the ellipsometry models given in Figure 7.

Figure 4 depicts the experimental and best fitted spectra of ψ and Δ and Figure 5 gives the experimental and calculated values for the “global” refractive index for all the samples: single oxide layers and three layers oxide/metal/oxide films deposited on glass substrates. The optimization of the models was done by comparing the calculated transmittance coefficient from ellipsometry model with the experimental values obtained from spectrophotometry (Figure 6). From curves given in Figure 4 and Figure 5, we remark a very good fit between the calculated data (lines) and experimental values (dots) but the optimization was done on the basis of successive comparison with the transmittance spectra obtained by spectrophotometry. Figure 6 presents the best fits of the calculated transmittance spectra from ellipsometry with transmittance spectra obtained by spectrophotometry.

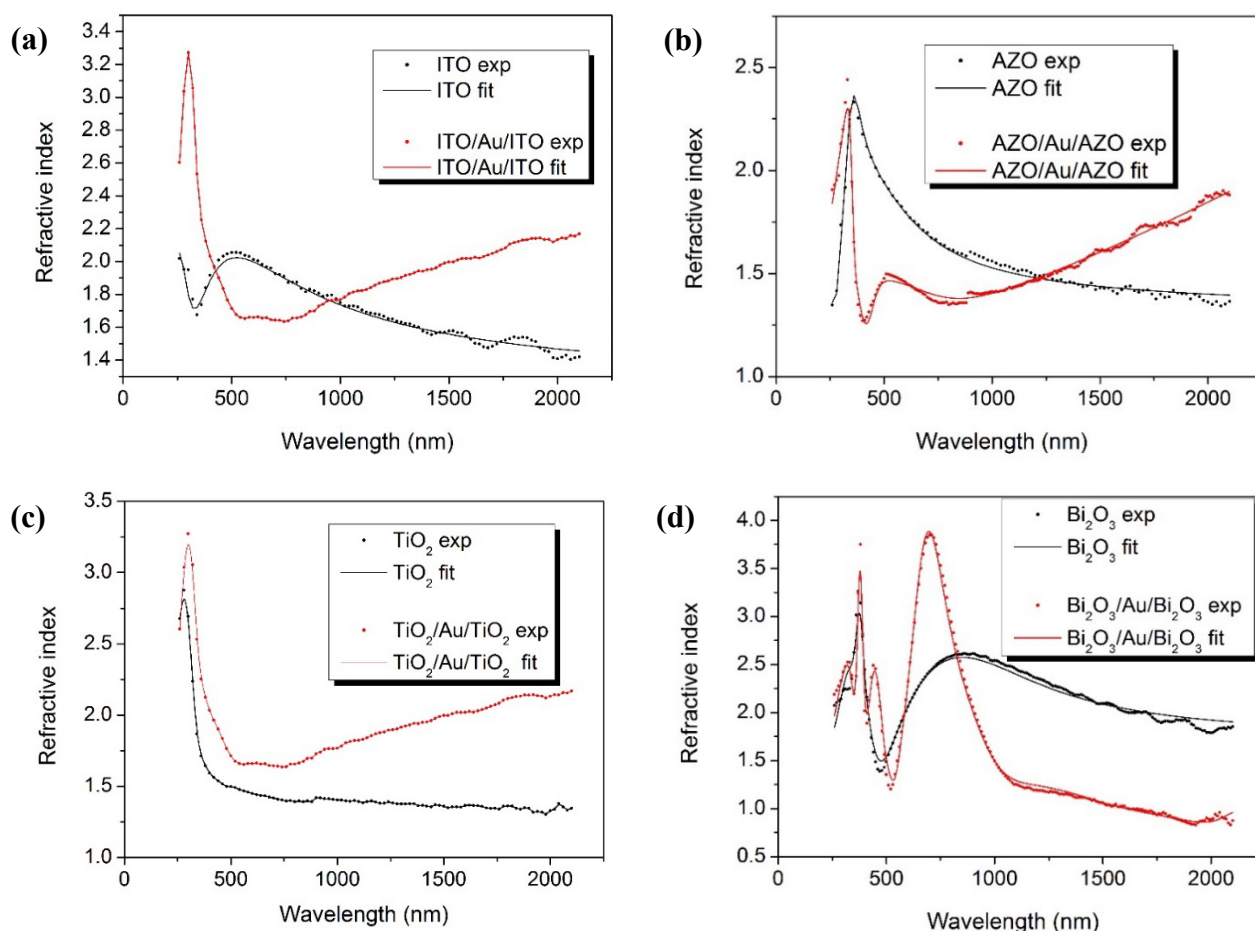


Figure 5. Samples global refractive index n , for single layer oxide on glass and three layers oxide/metal/oxide layers on glass substrate (experimental—dots and fit—line).

If the thickness d of a film, its refractive index n , and extinction coefficient k are known, it is possible to derive its reflectance R and transmittance T . Basic equations have been derived by Heavens [48] and are detailed for a single layer on a substrate of refractive index n_I and extinction coefficient k_I in [49]. In the same way calculations can be made for samples with multiple layers. A computer solution can also be carried out by successive approximations using Newton’s method [3,49,50]. The DeltaPsi2 software allows such calculations and gives the values of the transmission and reflection coefficients.

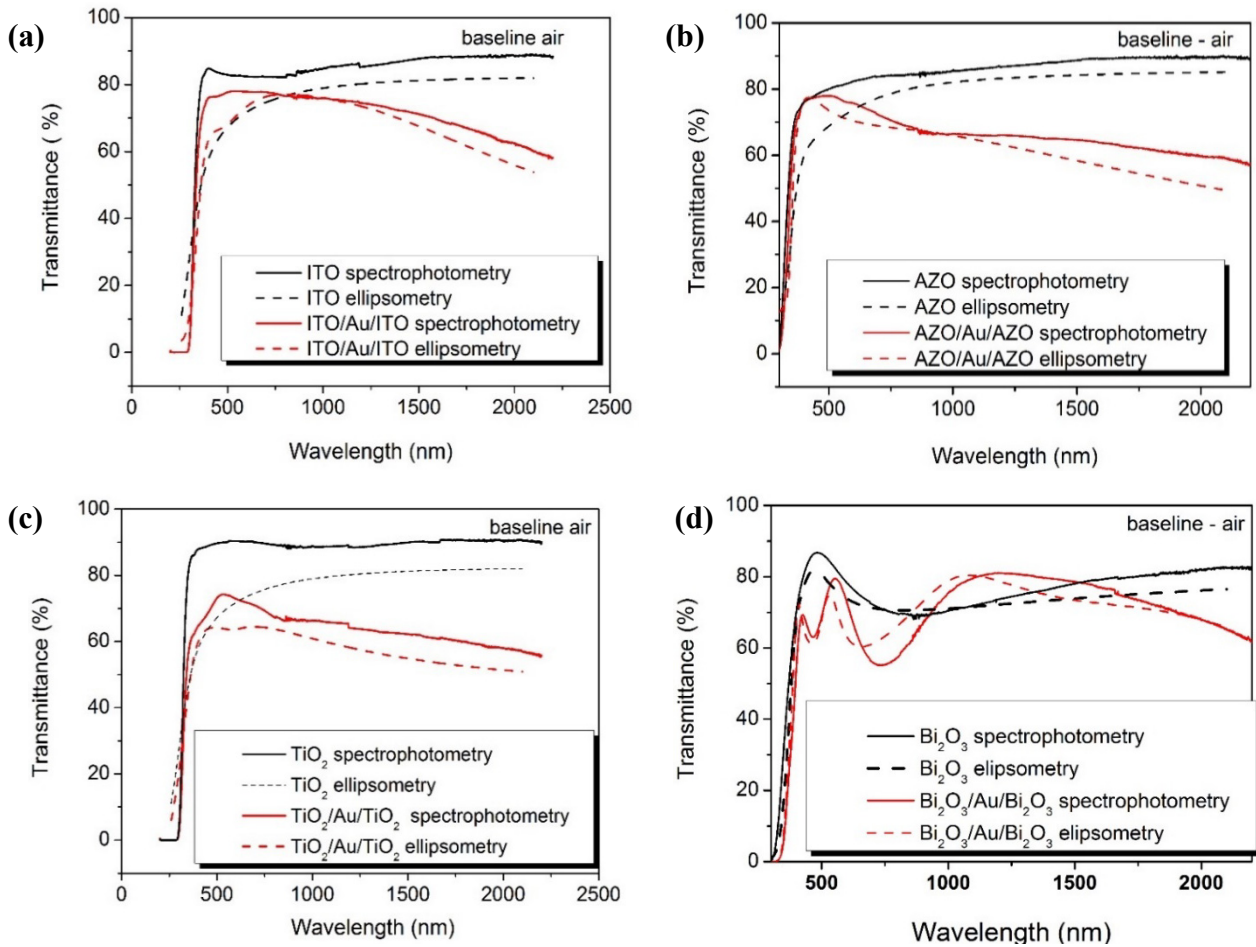


Figure 6. Transmission coefficient from spectrophotometric experimental data and ellipsometric calculations models for single and three layers samples.

Figure 7 indicates the dispersion models used in each case. The formulas of dispersion models are: based on the sum of the single and double Lorentz and Drude classical oscillators for ITO films, in agreement with [51,52,53]:

$$\varepsilon = \varepsilon_{\infty} + \frac{(\varepsilon_s - \varepsilon_{\infty})\omega_t^2}{\omega_t^2 - \omega^2 + i\Gamma_0\omega} + \frac{\omega_p^2}{-\omega^2 + i\Gamma_D\omega} + \sum_{j=1}^2 \frac{f_j\omega_{0j}^2}{\omega_{0j}^2 - \omega^2 + i\gamma_j\omega} \quad (7)$$

In agreement with [54] the best dispersion model founded for Al:ZnO doped films corresponds to Kato-Adachi dispersion model:

$$\varepsilon = \varepsilon_{\infty} + \varepsilon_1 + \varepsilon_2 + \varepsilon_3 + \varepsilon_4$$

$$\varepsilon_1 = \frac{A_0}{E_0^{1.5}} \cdot \frac{2 - \sqrt{1 + \chi} - \sqrt{1 - \chi}}{\chi^2}$$

$$\varepsilon_2 = -\frac{B_1}{\xi^2} \cdot \ln(1 - \xi^2)$$

$$\varepsilon_3 = \frac{B_1 \cdot X}{E_1 - E - i \cdot \Gamma_1}$$

$$\varepsilon_4 = \frac{C}{1 - \left(\frac{E}{E_2}\right)^2 - i \cdot \frac{E}{E_2} \cdot \Gamma_2}$$

$$\chi = \frac{E + i \cdot \Gamma_0}{E_0} \quad (8)$$



Figure 7. Ellipsometric models.

The new amorphous dispersion formula for TiO₂ is a rewriting of original Forouhi-Bloomer formula [55]:

$$n(\omega) = n_{\infty} + \frac{B \cdot (\omega - \omega_j) + C}{(\omega - \omega_j)^2 + \Gamma_j^2}$$

$$k(\omega) = \begin{cases} \frac{f_j \cdot (\omega - \omega_g)^2}{(\omega - \omega_j)^2 + \Gamma_j^2}, & \omega > \omega_g \\ 0, & \omega \leq \omega_g \end{cases}$$

where

$$B = \frac{f_j}{\Gamma_j} \cdot [\Gamma_j^2 - (\omega_j - \omega_g)^2]$$

$$C = 2 \cdot f_j \cdot \Gamma_j \cdot (\omega_j - \omega_g) \quad (9)$$

Tauc-Lorentz for Bi₂O₃ films [50,51]:

$$\varepsilon = \varepsilon_1 + \varepsilon_2 \quad \text{where:}$$

$$\varepsilon_2 = \begin{cases} \frac{1}{E} \cdot \frac{A \cdot E_0 \cdot C \cdot (E - E_g)^2}{(E^2 - E_0^2)^2 + C^2 \cdot E^2}, & E > E_g \\ 0, & E \leq E_g \end{cases}$$

$$\varepsilon_1 = \varepsilon_{\infty} + \frac{2}{\pi} \cdot P \cdot \int_{E_g}^{\infty} \frac{\xi \cdot \varepsilon_2(\xi)}{\xi^2 - E^2} d\xi \quad (10)$$

Drude:

$$\varepsilon = \frac{\omega_p^2}{-\omega^2 + i\Gamma_D \omega} \quad (11)$$

The dispersion models parameters corresponding hence to the best fit of the experimental data are given in Tables 2–6.

Table 2. Ellipsometric fitting parameters for ITO films.

Sample	Layer ITO/Dispersion model: double Lorentz + Drude						χ^2
	ε_{∞}	ε_s	ω_t	ω_p	Γ_0	Γ_d	
ITO	2.21	3.08	5.45	0.51	1.64	-0.37	4.57
ITO/Au/ITO	2.23	3.38	3.96	1.85	6.64	0.60	7.35

Table 3. Ellipsometric fitting parameters for AZO films.

Sample	Layer AZO/Dispersion model: Kato-Adachi											χ^2
	ϵ_∞	E_0 (eV)	A_0 (eV)	Γ_0 (cm^{-1})	E_1 (eV)	B_1 (eV)	$B_1 \cdot X$	Γ_1 (cm^{-1})	E_2 (eV)	C (eV)	Γ_2 (cm^{-1})	
AZO	4.86	2.09	20.70	1.08	3.71	1.78	0.33	0.26	6.65	3.72	-0.48	1.42
AZO/Au/AZO	1.54	3.31	13.05	-0.001	3.49	0.15	0.59	0.37	5.90	2.53	2.38	3.98

Table 4. Ellipsometric fitting parameters for TiO₂ films.

Sample	Layer TiO ₂ /Dispersion model: New Amorphous					χ^2
	n_∞	ω_g	f_j	ω_j	Γ_j	
TiO ₂	1.18	3.58	0.91	3.95	0.80	0.56
TiO ₂ /Au/TiO ₂	1.59	3.67	0.56	4.85	0.89	3.51

Table 5. Ellipsometric fitting parameters for Bi₂O₃ films.

Sample	Layer Bi ₂ O ₃ /Dispersion model: Tauc-Lorentz						χ^2
	Osc.	E_g (eV)	ϵ_∞	A (eV)	E_0 (eV)	C (eV)	
Bi ₂ O ₃	1	3.08	2.60	120.13	3.68	1.54	15.39
Bi ₂ O ₃ /Au/Bi ₂ O ₃	1	3.17	2.48	138.39	3.79	1.67	6.38

Table 6. Ellipsometric fitting parameters for Au films.

Sample	Layer Au/Dispersion model: Tauc-Lorentz + Drude								χ^2
	Osc.	E_g (eV)	n_∞	A (eV)	E_0 (eV)	C (eV)	ω_p (cm^{-1})	Γ (cm^{-1})	
ITO/Au/ITO	1	3.16	2.4	-958	3.06	0.26	14.18	-35.56	7.35
	2			182	2.25	11.45			
	3			32.96	-518	-4374			
AZO/Au/AZO	1	1.96	1.9	15.65	4.22	0.92	7.42	3.12	3.98
	2			-148.89	2.11	12.50			
	3			3.56	3.84	0.33			
TiO ₂ /Au/TiO ₂	1	2.26	2.01	233.51	2.27	0.203	6.10	0.172	3.51
	2			94.25	2.14	12.52			
	3			-74.47	-3.41	27.85			
Bi ₂ O ₃ /Au/Bi ₂ O ₃	1	1.60	3.16	8.14	1.65	-1.06	5.29	0.10	6.38
	2			279.50	2.12	12.65			
	3			40.59	3.92	-4.23			

Table 7 gives the thickness values for single and three layer samples. We remark a good correlation between the values obtained by profilometry and ellipsometry for the samples for which the transmission curves in Figure 6 (ITO/Au/ITO, AZO and Bi₂O₃) obtained by the two techniques are closer.

Table 7. Thin films thickness values determined by profilometry measurements and ellipsometry calculations.

No.	Sample	d (nm)		χ^2
		profilometry	ellipsometry	
1	ITO	45 ± 2	86 ± 2	4.57
2	AZO	40 ± 2	46 ± 3	1.42
3	TiO ₂	25 ± 2	17 ± 3	0.56
4	Bi ₂ O ₃	120 ± 2	124 ± 2	15.39
5	ITO/Au/ITO	45 ± 2/7 ± 2/45 ± 2	45 ± 2/9 ± 2/43 ± 3	7.35
6	AZO/Au/AZO	40 ± 2/10 ± 2/40 ± 2	27 ± 1/14 ± 2/22 ± 1	3.98
7	TiO ₂ /Au/TiO ₂	30 ± 2/7 ± 2/30 ± 2	21 ± 8/3 ± 2/16 ± 3	3.51
8	Bi ₂ O ₃ /Au/Bi ₂ O ₃	120 ± 2/10 ± 2/120 ± 2	141 ± 3/7 ± 1/149 ± 2	6.38

As confirmed, ellipsometry analysis is performed from fitting using an optical model. Nevertheless, an optical model used in ellipsometry analysis simply represents an approximated sample structure, and obtained results are not necessarily correct even when the fit is sufficiently good. This is the greatest disadvantage of the ellipsometry technique and accordingly, ellipsometry results must be justified by using other measurement methods [50]. The novelty of this paper consist in refining the modelling of optical properties by additionally fitting the transmission coefficients by two different techniques, moreover than the usual method presented in literature, which consist only on the fit of experimental ψ and Δ angles. By this deeper analysis of the optical models we can see that even after refining by this procedure and very good fits of ψ and Δ angles, or effective n and k coefficients, the fits for transmission coefficients by comparing the data from ellipsometry and spectrophotometry are not perfect. The differences observed between the transmission coefficient curves obtained by ellipsometry calculations and direct spectrophotometry measurements in Figure 6. for ITO, TiO₂ or Bi₂O₃/Au/Bi₂O₃ are coherent with the differences observed between the thickness values measured directly by profilometry and those calculated from ellipsometry and indicate the limits the optical models. However, once an analytical method is established, it becomes possible to perform high-precision characterization using spectroscopic ellipsometry. From this study, it can be considered that a good optical model can be established when the calculated curves of transmission coefficient obtained by ellipsometry coincides with the experimental values obtained by spectrophotometry and not only when good fits between experimental data and calculated values are obtained for the angles ψ and Δ angles, or effective n and k coefficients. The parameter which is most critically subject of errors, in the case of ellipsometry models calculations, is the films thickness, especially in the case of very thin films.

The dispersion curves of n and k of single layer oxides were extracted from these models and depicted in Figure 8.

The obtained values are in good agreement with the data obtained by other authors for ITO [56], AZO [57], TiO₂ [58] and Bi₂O₃ [59].

The absorption coefficient was calculated using the formula [3]:

$$\alpha(\lambda) = \frac{1}{d} \ln \left[\frac{1 - R(\lambda)}{T(\lambda)} \right] \quad (12)$$

The plot of $(h\nu\alpha)^n$ versus photon energy gives information about energy of the indirect ($n = 1/2$) or direct transitions ($n = 2$), respectively. By using the Eq. (12):

$$\alpha(h\nu) = \frac{A}{h\nu} (h\nu - E_g)^{1/n} \quad (13)$$

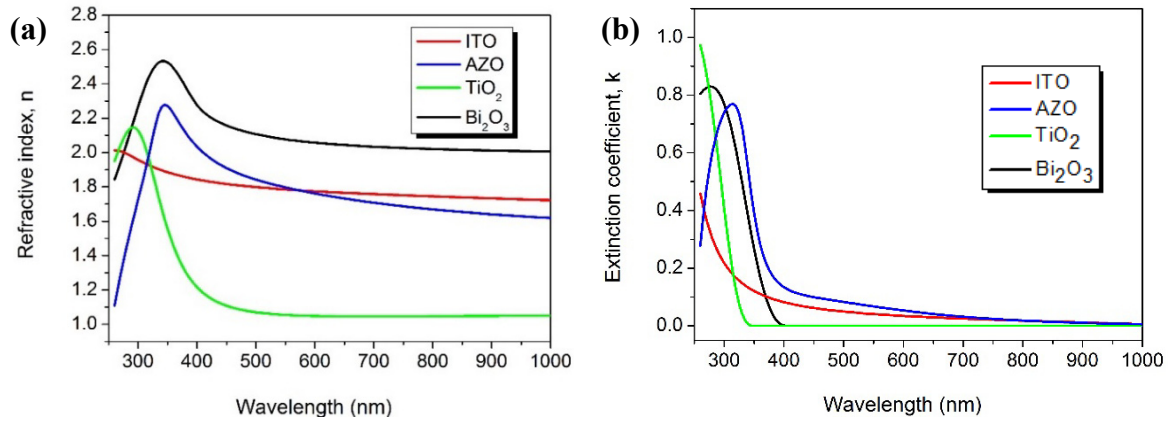


Figure 8. Refractive index and extinction coefficient for single oxide films.

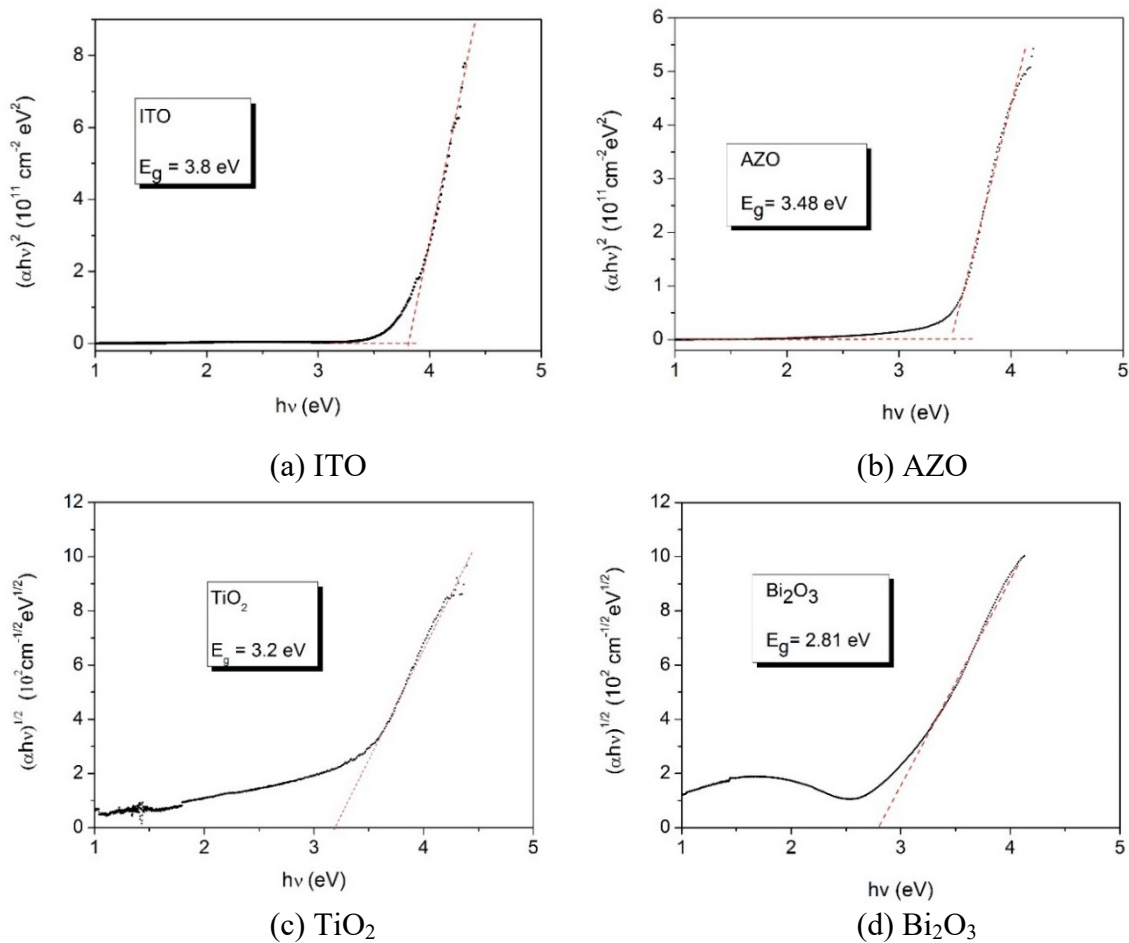


Figure 9. Optical gap calculations from spectrophotometry measurements.

For the direct allowed transition, $(h\nu\alpha)^2$ versus photon energy, $h\nu$ was plotted for ITO and AZO (Figure 9a and 9b). The intercept on the abscissa gives the value of the direct band gap [3]. The optical band gap values obtained (eV) are very close to the values quoted in literature [3,9].

The values for indirect band transitions for TiO_2 [60] and Bi_2O_3 [61] were determined from the linear extrapolation of $(h\nu\alpha)^{1/2} = f(h\nu)$ curves towards the intersection with the x-axis (Figure 9c and 9d).

The values of the optical band gaps determined from spectrophotometry data and ellipsometry calculations are given in Table 8. Good correlations between the calculations by the two methods were obtained.

Table 8. Oxide thin films optical band gap values determined by spectrophotometry measurements and ellipsometry calculations.

No.	Sample	E_g (eV)	E_g (eV)
		Spectrophotometry	Ellipsometry
1	ITO	3.80	4.20
2	AZO	3.48	3.48
3	TiO_2	3.20	3.58
4	Bi_2O_3	2.81	3.08

Single oxide layers films are high resistive due to the size effect as a consequence of their low thickness. The oxide/Au/oxide films have a good electrical conductivity due to the Au interlayer film. The electrical resistivity is of $8 \times 10^{-4} \Omega \cdot \text{cm}$ for ITO/Au/ITO, $2 \times 10^{-3} \Omega \cdot \text{cm}$ for AZO/Au/AZO, $7 \times 10^{-3} \Omega \cdot \text{cm}$ for $\text{TiO}_2/\text{Au}/\text{TiO}_2$, $3 \times 10^{-2} \Omega \cdot \text{cm}$ for $\text{Bi}_2\text{O}_3/\text{Au}/\text{Bi}_2\text{O}_3$.

The total (sheet) resistance of the multi-layer is a combination of the resistances of three consecutive layers [62]:

$$\frac{1}{R} = \frac{1}{R_{ox}} + \frac{1}{R_m} + \frac{1}{R_{ox}} \quad (14)$$

Hence:

$$R = \frac{R_{ox}R_m}{R_{ox} + 2R_m} = \frac{R_m}{1 + 2\frac{R_m}{R_{ox}}} \quad (15)$$

If we note $p = R_m/R_{ox}$

$$R = \frac{R_m}{1 + 2p} \quad (16)$$

Generally $R_{ox} \gg R_m \Rightarrow p \rightarrow 0 \Rightarrow$

$$R \cong R_m \quad (17)$$

According to Drude's theory in metals the plasma frequency is given by [63]:

$$\omega_p^2 = \frac{4\pi n e^2}{\epsilon_0 \epsilon_\infty m_e^*} \quad (18)$$

where n is the carriers concentration, m_e^* is the effective mass of charge carriers, ε_∞ and ε_0 represent the dielectric constants of medium and free space. On the other hand the electrical conductivity is given by:

$$\sigma = \frac{ne^2\langle\tau\rangle}{m_e^*} \quad (19)$$

where $\langle\tau\rangle$ is the mean value of the relaxation time, hence from the Eq. (18) and Eq. (19) it results that:

$$\omega_p^2 = \frac{4\pi\sigma}{\varepsilon_0\varepsilon_\infty\langle\tau\rangle} \quad (20)$$

Figure 10 presents the values of ω_p^2 obtained from the ellipsometric models (see Table 6) in function of the measured electrical conductivity in direction parallel to the substrate for the oxide/metal/oxide samples. We remark a linear dependence in agreement with Eq. (20). The resistance of single oxide layer of TiO_2 and Bi_2O_3 is higher than the resistance of individual ITO and AZO layers. In conclusion, the condition $R_{ox} \gg R_m$ is better verified for $\text{TiO}_2/\text{Au}/\text{TiO}_2$ and $\text{Bi}_2\text{O}_3/\text{Au}/\text{Bi}_2\text{O}_3$ which is coherent with the fact that for these samples the points (ω_p^2, σ) are closer to the linear dependence expressed by Eq. (20).

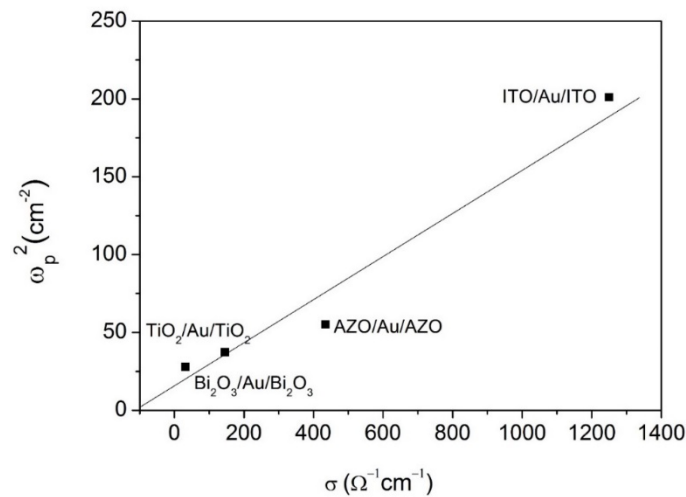


Figure 10. The values of ω_p^2 ($\omega_p = 2\pi f_p$, f_p —plasma frequency) obtained from the ellipsometric models (Table 6) in function of the measured electrical conductivity in direction parallel to the substrate for the oxide/metal/oxide samples.

4. Conclusions

A complete study of the optical and electrical properties of single oxide layer and oxide/metal/oxide (Oxide = ITO, AZO, TiO_2 and Bi_2O_3 , Metal = Au) three layers was done by spectrophotometry, ellipsometry and four probe electrical measurements. At our best knowledge, the multi-layer structure $\text{Bi}_2\text{O}_3/\text{Au}/\text{Bi}_2\text{O}_3$ was studied for the first time. Oxide films were deposited by reactive sputtering and all are amorphous and have a transmission coefficient higher than 80%. The improvement of the developed optical models was done by refining the fittings, not only, between the measured and the calculated values for the ψ and Δ angles, but also by comparing the calculated

values of the transmission coefficient from ellipsometric models with the experimental values of the transmission coefficient determined from spectrophotometry, and also by other correlations of specific parameters measured by other methods. This procedure allows to better establish the validity of the different optical models in function of the correlations obtained for different thin films characteristics such as the films thickness, transmission coefficient, optical band gap and electrical resistivity obtained by different techniques. The best dispersion models for $n(\lambda)$ and $k(\lambda)$ were hence established by the correlations of data obtained by spectrophotometry and ellipsometry. The global and individual refractive index and global and individual extinction coefficients were calculated. This approach also shows how the ellipsometric modelling can be improved, with maybe the possibility, in the future to predict, by ellipsometric simulations, the suitable device architecture in function of the desired optical and electrical properties.

Conflict of Interest

The authors declare that there is no conflict of interest regarding the publication of this manuscript.

References

1. Granqvist CG (2007) Transparent Conductors as Solar Energy Materials: A Panoramic Review. *Sol Energ Mat Sol C* 91: 1529–1598.
2. Granqvist CG (2003) Solar Energy Materials. *Adv Mater* 15: 1789–1803.
3. Girtan M (2005) Investigations on the Optical Constants of Indium Oxide Thin Films Prepared by Ultrasonic Spray Pyrolysis. *Mater Sci Eng B* 118: 175–178.
4. Girtan M, Folcher G (2003) Structural and optical properties of indium oxide thin films prepared by an ultrasonic spray CVD process. *Surf Coat Tech* 172: 242–250.
5. Girtan M, Rusu GI, Rusu GG (2000) The influence of preparation conditions on the electrical and optical properties of oxidized indium thin films. *Mater Sci Eng B* 76: 156–160.
6. Rusu M, Rusu GG, Girtan M, et al. (2008) Structural and optical properties of ZnO thin films deposited onto ITO/glass substrates. *J Non-Cryst Solids* 354: 4461–4464.
7. Girtan M, Bouteville A, Rusu GG, et al. (2006) Preparation and properties of SnO₂:F thin films. *J Optoelectron Adv M* 8: 27–30.
8. Girtan M, Vlad A, Mallet R, et al. (2013) On the properties of aluminium doped zinc oxide thin films deposited on plastic substrates from ceramic targets. *Appl Surf Sci* 274: 306–313.
9. Girtan M, Kompitsas M, Mallet R, et al. (2010) On physical properties of undoped and Al and In doped zinc oxide films deposited on PET substrates by reactive pulsed laser deposition. *Eur Phys J Appl Phys* 51.
10. Ghomrani FZ, Iftimie S, Gabouze N, et al. (2011) Influence of Al doping agents nature on the physical properties of Al:ZnO films deposited by spin-coating technique. *Optoelectron Adv Mat* 5: 247–251.
11. Socol M, Preda N, Rasoga O, et al. (2016) Flexible Heterostructures Based on Metal Phthalocyanines Thin Films Obtained by MAPLE. *Appl Surf Sci* 374: 403–410.

12. Girtan M, Mallet R, Caillou D, et al. (2009) Thermal Stability of Poly(3,4-ethylenedioxythiophene)-polystyrenesulfonic Acid Films Electric Properties. *Superlattice Microst* 46: 44–51.
13. Koralli P, Varol SF, Kompitsas M, et al. (2016) Brightness of Blue/Violet Luminescent Nano-Crystalline AZO and IZO Thin Films with Effect of Layer Number: For High Optical Performance. *Chinese Phys Lett* 33.
14. Iftimie S, Mallet R, Merigeon J, et al. (2015) On the structural, morphological and optical properties of ITO, ZnO, ZnO:Al and NiO thin films obtained by thermal oxidation. *Dig J Nanomater Bios* 10: 221–229.
15. Gong L, Lu JG, Ye ZZ (2011) Transparent conductive Ga-doped ZnO/Cu multilayers prepared on polymer substrates at room temperature. *Sol Energ Mat Sol C* 95: 1826–1830.
16. Girtan M, Mallet R (2014) On the electrical properties of transparent electrodes. Proceedings of the Romanian Academy Series A-Mathematics Physics Technical Sciences Information Science, 15: 146–150.
17. Girtan M (2012) Comparison of ITO/metal/ITO and ZnO/metal/ZnO Characteristics as Transparent Electrodes for Third Generation Solar Cells. *Sol Energ Mater Sol C* 100: 153–161.
18. Kubis P, Lucera L, Machui F, et al. (2014) High Precision Processing of Flexible P3HT/PCBM Modules with Geometric Fill Factor over 95%. *Org Electron* 15: 2256–2263.
19. Berny S, Blouin N, Distler A, et al. (2016) Solar Trees: First Large-Scale Demonstration of Fully Solution Coated, Semitransparent, Flexible Organic Photovoltaic Modules. *Adv Sci* 3.
20. Wanga K, Chenga B, Wub B, et al. (2014) Study of annealing effects upon the optical and electrical properties of SnO₂:F/SiC_xO_y low emissivity coatings by spectroscopic ellipsometry. *Thin Solid Films* 571: 720–726.
21. Yuan G, Wang K, Li M, et al. (2016) In situ optical characterizations of the annealing effects upon SnO₂:F films by spectroscopic ellipsometry. *Mater Res Express* 3: 105048.
22. Girtan M, Socol M, Pattier B, et al. (2010) On the structural, morphological, optical and electrical properties of sol-gel deposited ZnO In films. *Thin Solid Films* 519: 573–577.
23. Rusu GG, Girtan M, Rusu M (2007) Preparation and characterization of ZnO thin films prepared by thermal oxidation of evaporated Zn thin films. *Superlattice Microst* 42: 116–122.
24. Fortunato E, Nunes P, Marques A, et al. (2002) Transparent, conductive ZnO:Al thin film deposited on polymer substrates by RF magnetron sputtering. *Surf Coat Tech* 151: 247–251.
25. Craciun V, Amirhaghi S, Craciun D, et al. (1995) Effects of laser wavelength and fluence on the growth of ZnO thin-films by pulsed-laser deposition. *Appl Surf Sci* 86: 99–106.
26. Kim H, Horwitz JS, Kim WH, et al. (2002) Doped ZnO thin films as anode materials for organic light-emitting diodes. *Thin Solid Films* 420: 539–543.
27. Liu Y, Zhao L, Lian J (2006) Al-doped ZnO films by pulsed laser deposition at room temperature. *Vacuum* 81: 18–21.
28. Manole AV, Dobromir M, Girtan M, et al. (2013) Optical Properties of Nb-doped TiO₂ Thin Films Prepared by Sol-gel Method. *Ceram Int* 39: 4771–4776.
29. Saidi W, Hfaïdh N, Rashed M, et al. (2016) Effect of B₂O₃ Addition on Optical and Structural Properties of TiO₂ as a New Blocking Layer for Multiple Dye Sensitive Solar Cell Application (DSSC). *RSC Adv* 6: 68819–68826.
30. Mardare D, Iacomi F, Cornei N, et al. (2010) Undoped and Cr-doped TiO₂ thin films obtained by spray pyrolysis. *Thin Solid Films* 518: 4586–4589.

31. Vaiciulis I, Girtan M, Stanculescu A, et al. (2012) On titanium oxide spray deposited thin films for solar cells applications. Proceedings of the Romanian Academy Series A-Mathematics Physics Technical Sciences Information Science, 13: 335–342.
32. Mardare D, Yildiz A, Girtan M, et al. (2012) Surface wettability of titania thin films with increasing Nb content. *J Appl Phys* 112.
33. Pattier B, Henderson M, Kassiba A, et al. (2009) EPR and SAXS studies of a TiO₂-based gel. 3rd ICTON Mediterranean Winter Conference, Angers, France.
34. Green MA, HO-Baillie A, Snaith HJ (2014) The emergence of perovskite solar cells. *Nat Photonics* 8: 506–514.
35. Hagfeldt A, Cappel UB, Boschloo G, et al. (2012) Mesoporous Dye-Sensitized Solar Cells, Elsevier, 481–496.
36. Nazeeruddin MK, Grätzel M (2004) Conversion and Storage of Solar Energy using Dye-sensitized Nanocrystalline TiO₂ Cells, Pergamon, *Comprehensive Coordination Chemistry II*, 9: 719–758
37. Millington KR (2009) Photoelectrochemical cells|Dye-Sensitized Cells, *Encyclopedia of Electrochemical Power Sources*, 10–21.
38. Burschka J, et al. (2013) Sequential deposition as a route to high-performance perovskite-sensitized solar cells. *Nature* 499: 316–319.
39. Lee MM, Teuscher J, Miyasaka T, et al. (2012) Efficient hybrid solar cells based on meso-superstructured organometal halide perovskites. *Science* 338: 643–647.
40. Lewis NS (2004) Photosynthesis, Artificial, *Encyclopedia of Energy*, 17–24.
41. Pandit A, Frese RN (2012) Artificial Leaves: Towards Bio-Inspired Solar Energy Converters, In: Sayigh A, *Comprehensive Renewable Energy*, Elsevier, 657–677.
42. Rusu GI, Leontie L, Rusu GG, et al. (1999) On the electronic transport properties of oxidized bismuth thin films. *Analele Stiintifice Ale Universitatii Al. I. Cuza Din Iasi Fizica Stării Condensate* 104–112.
43. Fruth V, Popa M, Berger D, et al. (2005) Deposition and characterisation of bismuth oxide thin films. *J Eur Ceram Soc* 25: 2171–2174.
44. Tompkins HG, McGahan AW (1999) *Spectroscopic Ellipsometry and Reflectometry: A user's guide*, New York: Wiley.
45. Bhattacharyya D, Sahoo NK, Thakur S, et al. (2000) Spectroscopic ellipsometry of TiO₂ layers prepared by ion-assisted electron-beam evaporation. *Thin Solid Films* 360: 96–102.
46. Bernoux Fran F, Piel JP, Castellon B, et al. (2003) Ellipsométrie. Théorie. *Techniques de l'ingénieur. Mesures et contrôle* RD3: R6490.1–R6490.11.
47. Abeles F (1967) *Advanced Optical Techniques*, North-Holland, Amsterdam, 145.
48. Heavens OS (1955) *Optical Properties of Thin Solid Films*, London: Butter worth.
49. Hartnagel HL, Dawar AL, Jain AK, et al. (1995) *Semiconducting Transparent Thin Films*, Bristol: Institute of Physics.
50. Fujiwara H (2007) *Spectroscopic Ellipsometry: Principles and Applications*, New York: Wiley.
51. Horiba Delta Psi2 Software.
52. D'Elia S, Scaramuzza N, Ciuchi F. et al. (2009) Ellipsometry investigation of the effects of annealing temperature on the optical properties of indium tin oxide thin films studied by Drude–Lorentz model. *Appl Surf Sci* 255: 7203–7211.

53. Bellingham JR, Phillips WA, Adkins CJ (1991) Amorphous Indium Oxide. *Thin Solid Films* 202: 23–31.
54. Torres-Huerta M, Domínguez-Crespo MA, Brachetti-Sibaja SB, et al. (2011) Effect of the substrate on the properties of ZnO–MgO thin films grown by atmospheric pressure metal-organic chemical vapor deposition. *Thin Solid Films* 519: 6044–6052.
55. Forouhi AR, Bloomer I (1986) Optical dispersion relations for amorphous semiconductors and amorphous dielectrics. *Phys Rev B* 34: 7018.
56. Kim JK, Gessmann T, Schubert EF, et al. (2006) GaInN light-emitting diode with conductive omnidirectional reflector having a low refractive-index indium-tin oxide layer. *Appl Phys Lett* 88: 013501.
57. Wang YC, Lin BY, Liu PT, et al. (2013) Photovoltaic electrical properties of aqueous grown ZnO antireflective nanostructure on Cu(In, Ga)Se₂ thin film solar cells. *Opt Express* 22: A13–A20.
58. Mardare D, Hones P (1999) Optical dispersion analysis of TiO₂ thin films based on variable-angle spectroscopic ellipsometry measurements. *Mater Sci Eng B* 68: 42–47.
59. Condurache-Bota S, Tigau N, Rambu AP, et al. (2011) Optical and electrical properties of thermally oxidized bismuth thin films. *Appl Surf Sci* 257: 10545–10550.
60. Eiamchai P, Chindaudom P, Pokaipisit A, et al. (2009) A spectroscopic ellipsometry study of TiO₂ thin films prepared by ion-assisted electron-beam evaporation. *Curr Appl Phys* 9: 707–712.
61. Leontie L, Caraman M, Visinoiu A, et al. (2005) On the optical properties of bismuth oxide thin films prepared by pulsed laser deposition. *Thin Solid Films* 473: 230–235.
62. Sun HT, Wang XP, Kou ZQ, et al. (2015) Optimization of TiO₂/Cu/TiO₂ multilayers as a transparent composite electrode deposited by electron-beam evaporation at room temperature. *Chinese Phys B* 24: 047701.
63. Bube RH (1974) *Electronic Properties of Crystalline Solids*, New York: Academic Press.



AIMS Press

© 2017 Mihaela Girtan, et al., licensee AIMS Press. This is an open access article distributed under the terms of the Creative Commons Attribution License (<http://creativecommons.org/licenses/by/4.0>)